Acta Cryst. (1986). A42, 86-98

Nondiagonal Momentum Density of Si by Coherent Inelastic X-ray Scattering

BY W. SCHÜLKE AND S. MOURIKIS

Institut für Physik, Universität Dortmund, D4600 Dortmund 50, Federal Republic of Germany

(*Received* 19 *March* 1985; *accepted* 3 *September* 1985)

Abstract

When the coherent superimposition of two (nearly) plane waves is used as the initial photon state of an inelastic X-ray scattering experiment on solids (coherent Compton scattering), information can be obtained about the projection of nondiagonal elements of the one-particle density matrix in momentum space on the scattering vector **q**, provided the requirements of the impulse approximation are fulfilled. The double differential scattering cross section for this new scattering phenomenon is derived and then subjected to impulse approximation. It is further demonstrated that the standing wave pattern, which on passing the Bragg reflection range is sweeping the atomic sites, yields an appropriate approach to the desired initial photon state for coherent Compton scattering. Experimental coherent Compton spectra from 111 and 220 Bragg reflections are used to extract the corresponding projections of nondiagonal elements of the density matrix. Possible experimental improvements are discussed.

I. Introduction

The quantum-mechanical expectation value of a spin-independent single-particle quantity, as measured in a many-particle system, is generally determined by the complete spin-free one-particle density matrix, this means by both its diagonal and its nondiagonal elements (Löwdin, 1956). Moreover, within the limits of the Hartree–Fock approximation, the knowledge of the complete spin-free one-particle density matrix is sufficient for calculating expectation values of every spin-independent many-particle quantity, as measured in a many-particle system.

The diagonal elements of the position-space density matrix can be determined by means of X-ray diffraction measurements, provided the phase problem can be solved. The diagonal elements of the momentum-space density can be obtained by measuring directional Compton profiles and by applying appropriate momentum-space reconstruction methods (Mijnarends, 1977). It is well known (Benesch, Singh & Smith, 1971) that the measurement of diagonal elements of the density matrix in one space provides information about the space average of nondiagonal elements of the density matrix of the complementary space. So far, however, no experimental method is known that yields detailed information about nondiagonal elements of the spin-free one-particle density matrix in any space exceeding that that can be provided by measuring diagonal elements in two complementary spaces.

Most recently, it has been shown that, in principle, this type of detailed information can be obtained in momentum space by means of a special inelastic X-ray scattering experiment, where the coherent superimposition of two plane waves $\mathbf{K}_0$ and $\mathbf{K}_0+\mathbf{g}_h$ ($\mathbf{g}_h$ = reciprocal-lattice vector) is the initial photon state (coherent inelastic scattering) (Schülke, 1981; Golovchenko *et al.*, 1981; Schülke, Bonse & Mourikis, 1981; Schülke, 1982).

It will eludicate the physical significance of getting detailed information about nondiagonal density if one assumes that the ground state of the scattering system is represented by $\chi(\mathbf{p})$, a single-particle wave function in momentum space. In this case, conventional inelastic X-ray scattering, where only one plane wave represents the initial photon state, supplies information about $\chi(\mathbf{p})\chi^*(\mathbf{p})$, the momentum density. In this way one does not learn anything about the phase of $\chi(\mathbf{p})$. Coherent inelastic scattering, however, yields information about $\chi^*(\mathbf{p}+\mathbf{g}_h)\chi(\mathbf{p})$, the nondiagonal momentum density. By this means the relative phase of $\chi(\mathbf{p})$ can be measured. This can be seen in analogy to the phase problem of X-ray diffraction: When the incident wave satisfies the Bragg condition only for one set of planes, characterized by $\mathbf{g}_h$, one gets information only about $|F_h|$, the magnitude of the structure factor. By applying the coherent interaction among diffracted beams, which occur when two or more sets of planes diffract simultaneously, one can determine, in principle, the relative phases of the corresponding structure factors [see, for instance, the successful application of this method by Chang & Han (1982)]. It is the aim of this paper to derive first (§ II) the basic equations for the double differential cross section of inelastic scattering of photons from coherent wave fields in greater detail than in a previous publication (Schülke, 1981). In a second step (§ III) the application of the impulse approximation to these basic equations will lead to a relationship between the double differential inelastic scattering cross section and the nondiagonal elements of the one-particle density matrix in momentum space. In

0108-7673/86/020086-13$01.50

§ IV an experimental set up is proposed and discussed in detail, which makes possible inelastic scattering of photons from wave fields. In addition to a previous publication (Schülke, Bonse & Mourikis, 1981), the influences of detector resolution, beam divergences and polarization mixing on the final result are calculated in detail, and a method is proposed to prove the consistency of coherent Compton scattering results with conventional X-ray diffraction measurements. In § V, for the first time, experimental coherent inelastic scattering results in Si are used to derive information about nondiagonal matrix elements of the one-particle density matrix in momentum space, or, as far as the independent-particle model is concerned, information about the relative phases of momentum-space wave functions. Further improvements of experimental technique are discussed.

II. Double differential scattering cross section of coherent inelastic scattering

In conventional inelastic X-ray scattering experiments the initial photon state is simply a (nearly) plane wave. As will be shown in § IV, it is possible to realize experimentally the coherent superimposition of the two plane waves with wave vectors $\mathbf{K}_0$ and $\mathbf{K}_h = \mathbf{K}_0 + \mathbf{g}_h$ to be the initial photon state of an inelastic X-ray scattering experiment (coherent inelastic scattering). This can be done by setting a nearly perfect crystal into the Bragg position, where the dynamical theory of X-ray diffraction (Laue, 1960) predicts (within the limits of the two-beam approximation) a wave-field pattern, whose vector potential expectation value at the jth electron of the electron system under consideration can be written as follows:

$$\langle \mathbf{A}_j \rangle = (hc/2\omega_0)^{1/2}[A_0 \mathbf{e}_0 \cos(\mathbf{K}_0 \cdot \mathbf{r}_j) + A_h \mathbf{e}_h \cos(\mathbf{K}_h \mathbf{r}_j - \Delta\Phi)] \quad (2.1)$$

where $\mathbf{e}_0$ and $\mathbf{e}_h$ are the unit vectors of polarization of the $\mathbf{K}_0$- and $\mathbf{K}_h$-wave components, respectively.

Let the vector potential of the inelastically scattered wave be represented as in the conventional case by

$$\langle \mathbf{A}'_j \rangle = (hc/2\omega')^{1/2} A' \mathbf{e}' \cos(\mathbf{K}' \cdot \mathbf{r}_j). \quad (2.2)$$

It is easy to show that $\langle \mathbf{A}_j \rangle$ of (2.1) can be considered as the expectation value $\langle \Phi_i | \mathbf{A}_j | \Phi_i \rangle$ of the vector potential operator

$$\mathbf{A}_j \equiv (\pi\hbar c^2/\omega_0)^{1/2}\{\mathbf{e}_0[a_0^+ \exp(i\mathbf{K}_0 \cdot \mathbf{r}_j) + a_0 \exp(-i\mathbf{K}_0 \cdot \mathbf{r}_j)] + \mathbf{e}_h[a_h^+ \exp(i\mathbf{K}_h \cdot \mathbf{r}_j) + a_h \exp(-i\mathbf{K}_h \cdot \mathbf{r}_j)]\} \quad (2.3)$$

in the initial photon state

$$|\Phi_i\rangle = \sum_{n_0} |n_0\rangle (A_0^{2n_0} e^{-A_0^2}/n_0!)^{1/2} \times \sum_{n_h} |n_h\rangle (A_h^{2n_h} e^{-A_h^2}/n_h!) \times \exp[-i(n_h + 1/2)\,\Delta\Phi]|n'\rangle, \quad (2.4)$$

where $|n_0\rangle$, $|n_h\rangle$ and $|n'\rangle$ are energy eigenstates with n_0, n_h and n' photons in the mode, respectively. a^+ and a are creation and annihilation operators acting on photon fields. The total initial state of the system (photon field and scattering electron system) can be represented by

$$|I\rangle = |i\rangle|\Phi_i\rangle \quad (2.5)$$

where $|i\rangle$ is the initial state of the electron system.

In order to calculate the transition probability P in a coherent inelastic X-ray scattering experiment within the limits of first-order perturbation theory (Heitler, 1949), the final state $|F\rangle$ of the system has to be an energy eigenstate of the unperturbed Hamiltonian so that it can be written as

$$|F\rangle = |f\rangle|n_0\rangle|n_h\rangle|n'+1\rangle \quad (2.6)$$

with an additional photon in the $\mathbf{A}'$ field. $|f\rangle$ is the final state of the electron system. Within the limits of first-order perturbation theory, only that part of the interaction Hamiltonian

$$H_{\text{int}} = \sum_j (e/mc)\mathbf{A}_j \cdot \mathbf{p}_j + \sum_j (e^2/2mc^2)\mathbf{A}_j^2 \quad (2.7)$$

that is quadratic in the vector potential operator $\mathbf{A}_j$ contributes to the corresponding transition probability.

By expanding the initial state $|I\rangle$ into eigenstates

$$|L\rangle \equiv |l\rangle|m_0\rangle|m_h\rangle|m'\rangle \quad (2.8)$$

of the unperturbed Hamiltonian, the transition probability P reads as follows:

$$P = \left| \sum_{l,m_0,m_h,m'} \langle F|H_{\text{int}}|L\rangle\langle L|I\rangle \times \{-2i \exp[i(E_F - E_L)(t/2\hbar)] \times \sin[(E_F - E_L)(t/2\hbar)]/(E_F - E_L)\} \right|^2 \quad (2.9)$$

with

$$H_{\text{int}} = \sum_j (e^2/2mc^2)(\mathbf{A}_j + \mathbf{A}'_j)^2, \quad (2.10)$$

where $\mathbf{A}_j$ is given by (2.3) and

$$\mathbf{A}'_j = (\pi\hbar c^2/\omega_0)^{1/2}\{\mathbf{e}'[a'^+ \exp(i\mathbf{K}' \cdot \mathbf{r}_j) + a' \exp(-i\mathbf{K}' \cdot \mathbf{r}_j)]\} \quad (2.11)$$

according to (2.2).

The matrix elements of (2.9) can then be calculated as follows:

$$\langle F|H_{\text{int}}|L\rangle = [2e^2\pi\hbar/m(\omega_0\omega')^{1/2}](\mathbf{e}_0 \cdot \mathbf{e}') \times \langle f|\sum_j \exp[i(\mathbf{K}' - \mathbf{K}_0) \cdot \mathbf{r}_j]|l\rangle \times m_0^{1/2}(m'+1)^{1/2}\delta_{n_h,m_h}\delta_{n_0,m_0-1} + (\mathbf{e}_h \cdot \mathbf{e}_0)\langle f|\sum_j \exp[i(\mathbf{K}' - \mathbf{K}_h) \cdot \mathbf{r}_j]|l\rangle \times m_h^{1/2}(m'+1)^{1/2}\delta_{n_0,m_0}\delta_{n_h,m_h-1}\}\delta_{n'+1,m'+1} \quad (2.12)$$

and

$$\langle L|I\rangle = (A_0^{2m_0}e^{-A_0^2}/m_0!)^{1/2}(A_h^{2m_h}e^{-A_h^2}/m_h!)^{1/2} \times \exp[i(m_h+1/2)\Delta\Phi]\delta_{l,i}\delta_{m',n'}. \quad (2.13)$$

Insertion of (2.12) and (2.13) into (2.9) yields

$$\begin{aligned} P(t) = {} & (16\pi^2\hbar^2e^4/m^2\omega_0\omega')(A_0^{2n_0}e^{-A_0^2}/n_0!) \\ & \times (A_h^{2n_h}e^{-A_h^2}/n_n!)(n'+1)\{(\mathbf{e}_0\cdot\mathbf{e}')^2|\rho_{\mathbf{q}_0,f,i}|^2A_0^2 \\ & +(\mathbf{e}_h\cdot\mathbf{e}')^2|\rho_{\mathbf{q}_h,f,i}|^2A_h^2+(\mathbf{e}_0\cdot\mathbf{e}')(\mathbf{e}_h\mathbf{e}')A_0A_h \\ & \times[\rho_{\mathbf{q}_0,f,i}\rho^*_{\mathbf{q}_h,f,i}\,e^{i\Delta\Phi}+\rho^*_{\mathbf{q}_0,f,i}\rho_{\mathbf{q}_h,f,i}\,e^{-i\Delta\Phi}]\} \\ & \times\sin^2[(E_F-E_I)(t/2\hbar)]/(E_F-E_I)^2, \end{aligned} \quad (2.14)$$

where

$$\mathbf{q}_0\equiv\mathbf{K}'-\mathbf{K}_0;\ \mathbf{q}_h\equiv\mathbf{K}'-\mathbf{K}_h;\ \mathbf{q}_h=\mathbf{q}_0-\mathbf{g}_h;$$

and

$$\rho_{\mathbf{q},f,i}\equiv\langle f|\sum_j\exp(i\mathbf{q}\cdot\mathbf{r}_j)|i\rangle.$$

Since the double differential scattering cross section arises from $P(t)$ by the following relation

$$\begin{aligned} d^2\sigma/d(\hbar\omega)\,d\Omega = {} & [c(A_0^2+A_h^2]^{-1} \\ & \times\sum_F(2\pi c)^3\,\hbar^{-1}\omega'^2\,dP(t)/dt; \\ \omega = {} & \omega_0-\omega', \end{aligned} \quad (2.15)$$

one obtains finally the double differential cross section (DDCS) of coherent inelastic scattering:

$$\begin{aligned} d^2\sigma/d(\hbar\omega)\,d\Omega = {} & [e^4/m^2c^4(A_0^2+A_h^2)](\omega'/\omega_0) \\ & \times\sum_f\{(\mathbf{e}_0\cdot\mathbf{e}')^2A_0^2|\rho_{\mathbf{q}_0,f,i}|^2 \\ & +(\mathbf{e}_h\cdot\mathbf{e}')^2A_h^2|\rho_{\mathbf{q}_h,f,i}|^2 \\ & +(\mathbf{e}_0\cdot\mathbf{e}')(\mathbf{e}_h\cdot\mathbf{e}')A_0A_h \\ & \times[\rho_{\mathbf{q}_0,f,i}\rho^*_{\mathbf{q}_h,f,i}\,e^{i\Delta\Phi} \\ & +\rho^*_{\mathbf{q}_0,f,i}\rho_{\mathbf{q}_h,f,i}\,e^{-i\Delta\Phi}]\}\delta(E_f-E_i-\hbar\omega), \end{aligned} \quad (2.16)$$

where E_i and E_f refer to the energy of the initial and final states of the electron system, respectively.

III. Impulse approximation of the coherent inelastic scattering cross section

As in the case of conventional inelastic X-ray scattering the expression (2.16) for the DDCS of coherent inelastic scattering can be approximated in such a way that is contains only ground-state properties, provided the transferred energy $\hbar\omega$ is large compared with characteristic energies of the system (impulse approximation). As has been shown by Eisenberger & Platzman (1970), the essentials of the impulse approximation are as follows. (For the sake of clarity all the following relations refer to a one-electron system. The extension to many-electron systems is given at the end of this section.)

1. The final state of the scattering system is thought to be free-electron like with momentum eigenstates $|\mathbf{p}\rangle$.

2. The time t ($t\simeq\omega^{-1}$) of interaction during the inelastic scattering process is thought to be small so that the potential energy cancels in the difference between the final- and initial-state energies of the scattering system in the δ function of (2.16).

This type of approximation can be expressed in terms of quantum mechanics by noticing that, for a Hamiltonian $H=(2m)^{-1}p^2+V=H_0+V$,

$$\exp\{\tfrac{1}{2}[H_0,\,V]t^2/\hbar^2\}\simeq 1 \quad (3.1)$$

as long as only time intervals $t\lesssim\omega^{-1}$ are involved, and $\hbar\omega$ is large compared with characteristic energies of the scattering system. Following this line also for coherent inelastic scattering, one ends up with the following expression for the double differential scattering cross section as shown in Appendix A:

$$\begin{aligned} d^2\sigma/d\omega\,d\Omega = {} & [r_0^2/(A_0^2+A_h^2)](\omega'/\omega_0) \\ & \times\Bigg\{(\mathbf{e}_0\cdot\mathbf{e}')^2A_0^2\sum_{\mathbf{p}}|\langle i|\mathbf{p}\rangle|^2 \\ & \times\delta(\omega-\hbar q_0^2/2m-\mathbf{p}\cdot\mathbf{q}_0/m) \\ & +(\mathbf{e}_h\cdot\mathbf{e}')^2A_h^2\sum_{\mathbf{p}}|\langle i|\mathbf{p}\rangle|^2 \\ & \times\delta(\omega-\hbar q_h^2/2m-\mathbf{p}\cdot\mathbf{q}_h/m) \\ & +\tfrac{1}{2}(\mathbf{e}_0\cdot\mathbf{e}')(\mathbf{e}_h\cdot\mathbf{e}')A_0A_h \\ & \times\Bigg(e^{i\Delta\Phi}\Bigg[\sum_{\mathbf{p}}\langle i|\mathbf{p}+\mathbf{g}_h\rangle\langle\mathbf{p}|i\rangle \\ & \times\delta(\omega-\hbar q_0^2/2m-\mathbf{p}\cdot\mathbf{q}_0/m) \\ & +\sum_{\mathbf{p}}\langle i|\mathbf{p}\rangle\langle\mathbf{p}-\mathbf{g}_h|i\rangle \\ & \times\delta(\omega-\hbar q_h^2/2m-\mathbf{p}\cdot\mathbf{q}_h/m)\Bigg] \\ & +e^{-i\Delta\Phi}\Bigg[\sum_{\mathbf{p}}\langle i|\mathbf{p}-\mathbf{g}_h\rangle\langle\mathbf{p}|i\rangle \\ & \times\delta(\omega-\hbar q_h^2/2m-\mathbf{p}\cdot\mathbf{q}_h/m) \\ & +\sum_{\mathbf{p}}\langle i|\mathbf{p}\rangle\langle\mathbf{p}+\mathbf{g}_h|i\rangle \\ & \times\delta(\omega-\hbar q_0^2/2m-\mathbf{p}\cdot\mathbf{q}_0/m)\Bigg]\Bigg)\Bigg\}, \end{aligned} \quad (3.2)$$

where $r_0\equiv e^2/mc^2$.

The first two terms in the { } brackets of (3.2) contain the information about the diagonal momentum density of the ground state $|\langle i|\mathbf{p}\rangle|^2$ as in conventional Compton profiles, that is the projection of the diagonal momentum density on the scattering vectors $\mathbf{q}_0$ and $\mathbf{q}_h$, respectively. The third term (interference

term) provides the desired information on the projection of the nondiagonal momentum density, *e.g.* $\langle i|\mathbf{p}+\mathbf{g}_h\rangle\langle \mathbf{p}|i\rangle$, of the ground state on $\mathbf{q}_0$ and $\mathbf{q}_h$, respectively.

The interference term of (3.2) will further be reduced if $\mathbf{q}_0$ and $\mathbf{q}_h$ are equivalent with respect to the crystal symmetry. In this case the following equation holds:

$$\sum_{\mathbf{p}} \langle i|\mathbf{p}+\mathbf{g}_h\rangle\langle \mathbf{p}|i\rangle\delta(\omega-\hbar q_0^2/2m-\mathbf{p}\cdot\mathbf{q}_0/m) = \sum_{\mathbf{p}} \langle i|\mathbf{p}\rangle\langle \mathbf{p}-\mathbf{g}_h|i\rangle\delta(\omega-\hbar q_h^2/2m-\mathbf{p}\cdot\mathbf{q}_h/m) \quad (3.3)$$

provided that

$$q_0^2 = q_h^2 \equiv q^2. \quad (3.4)$$

Obviously, in these cases, the first two terms of (3.2) are identical. If, additionally, the expressions on the right-hand and left-hand sides of (3.3) are real valued, (3.2) reduces to

$$\begin{aligned} d^2\sigma/d\omega\, d\Omega = {} & [r_0^2/(A_0^2+A_h^2)](\omega'/\omega_0)(8\pi^3)^{-1} \\ & \times\{[(\mathbf{e}_0\cdot\mathbf{e}')^2A_0^2+(\mathbf{e}_h\cdot\mathbf{e}')^2A_h^2] \\ & \times\int d\mathbf{p}|\langle i|\mathbf{p}\rangle|^2\delta(\omega-\hbar q^2/2m-\mathbf{p}\cdot\mathbf{q}/m) \\ & +2(\mathbf{e}_0\cdot\mathbf{e}')(\mathbf{e}_h\cdot\mathbf{e}')A_0A_h\cos\Delta\Phi \\ & \times\int d\mathbf{p}\langle i|\mathbf{p}+\mathbf{g}_h\rangle \\ & \times\langle \mathbf{p}|i\rangle\delta(\omega-\hbar q^2/2m-\mathbf{p}\cdot\mathbf{q}/m)\}, \end{aligned} \quad (3.5)$$

where the summation with respect to $\mathbf{p}$ was replaced by an integration. The first integral in the { } brackets is the well known Compton profile. The second integral, which contains the information about the nondiagonal momentum density, should be called the 'nondiagonal profile'. Finally, the impulse approximation has to be extended to a many-particle system by introducing $\Gamma_1(\mathbf{p}|\mathbf{p}')$, the one-particle density matrix in momentum space (1 DMMS), together with the two-particle density matrix $\Gamma_2(\mathbf{p}_1,\mathbf{p}_2|\mathbf{p}_1',\mathbf{p}_2')$ in momentum space (2 DMMS) according to Löwdin's convention (Löwdin, 1956). This is performed in Appendix *B*, where it is shown that, for instance, the term

$$\left\langle f\left|\sum_j e^{i\mathbf{q}_0\cdot\mathbf{r}_j}\right|i\right\rangle\left\langle i\left|\sum_j e^{-i\mathbf{q}_h\cdot\mathbf{r}_j}\right|f\right\rangle\delta(E_f-E_i-\hbar\omega) \quad (3.6)$$

of (2.16) can be written as

$$\begin{aligned} & \tfrac{1}{2}\{\int d\mathbf{p}\Gamma_1(\mathbf{p}+\mathbf{g}_h|\mathbf{p})\delta(\omega-\hbar q_0^2/2m-\mathbf{p}\cdot\mathbf{q}_0/m) \\ & +\int d\mathbf{p}\,\Gamma_1(\mathbf{p}|\mathbf{p}-\mathbf{g}_h)\delta(\omega-\hbar q_h^2/2m-\mathbf{p}\cdot\mathbf{q}_h/m) \\ & +2\int d\mathbf{p}_1\,d\mathbf{p}_2\,\Gamma_2(\mathbf{p}_2-\mathbf{q}_h,\mathbf{p}_1+\mathbf{q}_0|\mathbf{p}_2,\mathbf{p}_1) \\ & \times\delta(\omega-\hbar\mathbf{q}_0^2/2m-\mathbf{p}_1\cdot\mathbf{q}_0/m) \\ & +2\int d\mathbf{p}_1\,d\mathbf{p}_2\,\Gamma_2(\mathbf{p}_2,\mathbf{p}_1|\mathbf{p}_2+\mathbf{q}_h,\mathbf{p}_1-\mathbf{q}_0) \\ & \times\delta(\omega-\hbar q_h^2/2m-\mathbf{p}_2\cdot\mathbf{q}_h/m)\}. \end{aligned} \quad (3.7)$$

As already pointed out by Benesch & Smith (1973), the third and fourth term of (3.7) can be neglected compared to the first and second ones under experimental conditions, which fit the impulse approximation.

Therefore, (3.2) can be written for many-electron systems as follows:

$$\begin{aligned} d^2\sigma/d\omega\, d\Omega = {} & [r_0^2/(A_0^2+A_h^2)](\omega'/\omega_0)\{(\mathbf{e}_0\cdot\mathbf{e}')^2A_0^2 \\ & \times\int d\mathbf{p}\,\Gamma(\mathbf{p}|\mathbf{p})\delta(\omega-\hbar q_0^2/2m-\mathbf{p}\cdot\mathbf{q}_0/m) \\ & +(\mathbf{e}_h\cdot\mathbf{e}')^2A_h^2\int d\mathbf{p}\,\Gamma(\mathbf{p}|\mathbf{p}) \\ & \times\delta(\omega-\hbar q_h^2/2m-\mathbf{p}\cdot\mathbf{q}_h/m) \\ & +\tfrac{1}{2}(\mathbf{e}_0\cdot\mathbf{e}')(\mathbf{e}_h\cdot\mathbf{e}')A_0A_h \\ & \times[e^{i\Delta\Phi}(\int d\mathbf{p}\,\Gamma(\mathbf{p}+\mathbf{g}_h|\mathbf{p}) \\ & \times\delta(\omega-\hbar q_0^2/2m-\mathbf{p}\cdot\mathbf{q}_0/m) \\ & +\int d\mathbf{p}\,\Gamma(\mathbf{p}|\mathbf{p}-\mathbf{g}_h) \\ & \times\delta(\omega-\hbar q_h^2/2m-\mathbf{p}\cdot\mathbf{q}_h/m)) \\ & +e^{-i\Delta\Phi}(\int d\mathbf{p}\,\Gamma(\mathbf{p}-\mathbf{g}_h|\mathbf{p}) \\ & \times\delta(\omega-\hbar q_h^2/2m-\mathbf{p}\cdot\mathbf{q}_h/m) \\ & +\int d\mathbf{p}\,\Gamma(\mathbf{p}|\mathbf{p}+\mathbf{g}_h) \\ & \times\delta(\omega-\hbar q_0^2/2m-\mathbf{p}\cdot\mathbf{q}_0/m))]\}, \end{aligned} \quad (3.8)$$

where the subscript 1 for the one-particle matrix has been dropped.

Equation (3.8) can further be reduced in the same way as in the one-electron case [(3.5)], provided $\mathbf{q}_0$ and $\mathbf{q}_h$ are crystal-symmetry equivalent:

$$\begin{aligned} d^2\sigma/d\omega\, d\Omega = {} & [r_0^2/(A_0^2+A_h^2)](\omega'/\omega_0) \\ & \times\{[(\mathbf{e}_0\cdot\mathbf{e}')^2A_0^2 \\ & +(\mathbf{e}_h\cdot\mathbf{e}')^2A_h^2]\mathcal{J}_{\mathbf{q},0}(Q) \\ & +2(\mathbf{e}_0\cdot\mathbf{e}')(\mathbf{e}_h\cdot\mathbf{e}')A_0A_h\cos(\Delta\Phi) \\ & \times\mathcal{J}_{\mathbf{q},\mathbf{g}_h}(Q)\}, \end{aligned} \quad (3.9)$$

where $\mathcal{J}_{\mathbf{q},0}(Q)$ denotes the Compton profile

$$\mathcal{J}_{\mathbf{q},0}(Q) \equiv \int d\mathbf{p}\,\Gamma(\mathbf{p}|\mathbf{p})\delta(\omega-\hbar q^2/2m-qQ/m) \quad (3.10a)$$

and $\mathcal{J}_{\mathbf{q},\mathbf{g}_h}(Q)$ denotes the nondiagonal profile

$$\mathcal{J}_{\mathbf{q},\mathbf{g}_h}(Q) \equiv \int d\mathbf{p}\,\Gamma(\mathbf{p}+\mathbf{g}_h|\mathbf{p})\delta(\omega-\hbar q^2/2m-qQ/m). \quad (3.10b)$$

Q is defined by

$$Q = \mathbf{p}\cdot\mathbf{q}/q = m\omega/q-\hbar q/2. \quad (3.11)$$

IV. Experimental realization of coherent inelastic scattering

According to (3.8) of the preceding section, one can obtain the desired information about the nondiagonal elements of the 1 DMMS by measuring the DDCS

for two different initial photon states, characterized by (A_{01}, $\mathbf{e}_{01}$, A_{h1}, $\mathbf{e}_{h1}$, $\Delta\Phi_1$) and (A_{02}, $\mathbf{e}_{02}$, A_{h2}, $\mathbf{e}_{h2}$, $\Delta\Phi_2$). These well defined initial photon states can be realized within a sample crystal by means of the following experimental setup (Fig. 1) utilizing the well known relations of X-ray optics for nearly perfect crystals.

The sample is the second crystal of a nondispersive double-crystal setting at the Bragg position, where the first crystal has to be cut asymmetrically in order to obtain an extremely well collimated beam at the second (sample) crystal. The sample crystal is enclosed within an evacuated scattering chamber. According to the well known relations of the dynamical theory of X-ray diffraction (Laue, 1960), two coherent plane waves, the Bragg-reflected wave A_h, $\mathbf{e}_{h'}$, $\mathbf{K}_h$, and the 'forward-diffracted' wave A_0, $\mathbf{e}_0$, $\mathbf{K}_0$ with $\mathbf{K}_h = \mathbf{K}_0 + \mathbf{g}_h$ are excited at the sample crystal, so that the amplitude ratio A_h/A_0 together with the mutual phase shift $\Delta\varphi$ of the two plane-wave components are mainly determined by y, the normalized deviation from the exact Bragg position *via* the following equations, which hold for the so-called Bragg case of diffraction (Bonse, 1964):

$$\begin{aligned}\xi^{(\nu)} &\equiv (A_h/A_0)\, e^{-i\Delta\Phi} \\ &= -(-1)^{\tau^{(\nu)}}(\gamma_0\chi_h/|\gamma_h|\chi_{\bar{h}})^{1/2} \\ &\quad \times (d\{1-[(E-1)/(E+1)]^{1/2}\} \\ &\quad + if\{1-[(E+1)/(E-1)]^{1/2}\}), \end{aligned} \tag{4.1}$$

with

$$E = d^2+f^2+[1+(d^2+f^2)-2(d^2-f^2)]^{1/2} \tag{4.2}$$

$$d \equiv (|\chi_{i0}|\Psi_h v/\Phi_h^{1/2}2\Phi_h|C|)+y;$$

$$f \equiv |\chi_{i0}|v/\Phi_h^{1/2}|C| - \Psi_h y/2\Phi_h \tag{4.3}$$

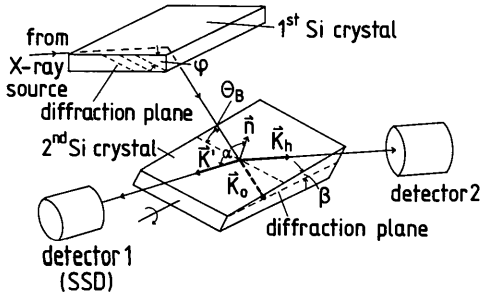

Fig. 1. Experimental nondispersive double-crystal setting. First crystal: asymmetrically cut crystal. φ is the angle between the crystal surface and the diffraction plane. Second crystal: the crystal surface is inclined by β from the diffraction plane so that the surface and the diffraction plane intersect along a line parallel to $\mathbf{K}_0+\mathbf{K}_h$. $\mathbf{n}$ is the normal to the crystal surface. The direction $\mathbf{K}'$ of the scattered wave has to be chosen so that $|\mathbf{K}'-\mathbf{K}_0| = |\mathbf{K}'-\mathbf{K}_h|$ and $\mathbf{K}'-\mathbf{K}_0$ is equivalent to $\mathbf{K}'-\mathbf{K}_h$ with respect to crystal symmetry. Detector 1 (solid-state detector) is the energy analyzer for the inelastically scattered beam. By means of detector 2 the rocking-curve intensity is measured in order to read and to keep constant the relative orientation of the two crystals.

$$\gamma_0 \equiv \cos\psi_0;\ \gamma_h \equiv \cos\psi_h \tag{4.4}$$

$$v \equiv \tfrac{1}{2}[(\gamma_0/|\gamma_h|)^{1/2}+(|\gamma_h|/\gamma_0)^{1/2}] \tag{4.5}$$

$$\tau = 1, \text{ if } C<0, \text{ otherwise } \tau = 0 \tag{4.6}$$

$$C = \begin{cases} \cos 2\theta_B & \text{if } \mathbf{e}_0 \text{ and } \mathbf{e}_h \text{ are within the plane of } \mathbf{K}_0 \text{ and } \mathbf{K}_h \\ 1 & \text{if } \mathbf{e}_0 \text{ and } \mathbf{e}_h \text{ are both perpendicular to the plane of } \mathbf{K}_0 \text{ and } \mathbf{K}_h \end{cases} \tag{4.7}$$

$$\beta_r \equiv 2(\psi_0-\psi_{0B})\sin 2\theta_\beta + |\chi_{r0}|(1+|\gamma_h|/\gamma_0) \tag{4.8}$$

$$\beta_i \equiv |\chi_{i0}|(1+|\gamma_h|/\gamma_0) \tag{4.9}$$

$$y \equiv \beta_r/(2C(|\gamma_h|/\gamma_0)^{1/2}\Phi_h^{1/2}) \tag{4.10}$$

$$\Phi_h \equiv \chi_{rh}\chi_{r\bar{h}} - \chi_{ih}\chi_{i\bar{h}};\ \Psi_h \equiv \chi_{rh}\chi_{i\bar{h}} + \chi_{r\bar{h}}\chi_{ih} \tag{4.11}$$

$$\psi_{0B} \equiv \pi/2 - \theta_B - \varphi, \tag{4.12}$$

where ψ_0 and ψ_h are the angles of the forward-diffracted and of the Bragg-reflected wave vector, respectively, with the crystal surface normal. χ_{rh} and χ_{ih} are the gth Fourier component of the real and imaginary parts of the dielectric susceptibility $\chi = \chi_r + i\chi_i$. φ is the angle between the crystal surface and the Bragg diffracting plane. θ_B is the Bragg angle. It should be kept in mind that y, the normalized deviation from the exact Bragg position (including the effect of refraction), depends on the polarization state of the two plane-wave components according to (4.9) together with (4.6). This polarization dependence of y also makes ξ, as defined in (4.1), polarization dependent. In order to draw attention to this polarization dependence, whenever it is of importance, ν indicates the components of $A_0\mathbf{e}_0$ and $A_h\mathbf{e}_h$ normal ($\nu = 1$) and parallel ($\nu = 2$) to the $\mathbf{K}_0$, $\mathbf{K}_h$ plane.

The wave field, composed of the two plane-wave components $A_0\mathbf{e}_0$, $\mathbf{K}_0$ and $A_h\mathbf{e}_h$, $\mathbf{K}_h$, is damped with an extinction coefficient σ in the direction of the sample surface normal, which is given by (Wagner, 1956)

$$\sigma(y) = (\mu/2)\{\gamma_0^{-1} - |\gamma_h|^{-1} \mp (|\chi_{i0}||\chi_h|)^{-1}\,\mathrm{Im}\ W\}, \tag{4.13}$$

where

$$\begin{aligned} W = [&\beta_r^2 - \beta_i^2 + 4C^2|\chi_{rh}|^2|\gamma_h|/\gamma_0 \\ &+ 2i(\beta_r\beta_i - 2C^2\Psi_h|\gamma_h|/\gamma_0)]^{1/2}. \end{aligned} \tag{4.14}$$

μ is the linear mass absorption coefficient for X-rays of the corresponding wavelength. y_{II}, the normalized deviation from the exact Bragg position of the sample crystal (second crystal of the double-crystal setup of Fig. 1) or, better, the effective range of y_{II}, is defined experimentally by $\bar{y}$, the angular position of the first crystal relative to the sample crystal, since the intensity $I(y_{\mathrm{I}})$, Bragg reflected at the first crystal, is limited to a small angular range of y_{I} according to

$$I(y_{\mathrm{I}}) \propto |\xi_{\mathrm{I}}(y_{\mathrm{I}})|^2. \tag{4.15}$$

Therefore, $\bar{y}$ can be monitored by measuring the rocking curve $I(\bar{y})$, that is the intensity, which is Bragg reflected by the second crystal of the nondispersive double-crystal setting given by

$$I(\bar{y}) = \tfrac{1}{2} I_0 \sum_{\nu=1}^{2} \int |\xi_{\mathrm{I}}^{(\nu)}(y_{\mathrm{I}}^{(\nu)} - \bar{y})|^2 |\xi_{\mathrm{II}}^{(\nu)}(B y_{\mathrm{I}}^{(\nu)})|^2 \, \mathrm{d}y_{\mathrm{I}}^{(\nu)}, \tag{4.16}$$

where

$$B = (|\gamma_h|/\gamma_0)_{\mathrm{I}}^{1/2} / (|\gamma_h|/\gamma_0)_{\mathrm{II}}^{1/2}. \tag{4.17}$$

Equation (4.16) refers to an unpolarized incident beam of intensity I_0.

By comparing experimental rocking curves $I(\bar{y})$, which are measured behind the second crystal by means of detector 2 (scintillation counter), with calculated ones, one can determine $\bar{y}$ experimentally for every relative position of the sample crystal. The direction $\mathbf{K}'$ of the inelastically scattered wave has to be fixed in such a way that (3.4) is valid. In order to prevent grazing emergence of $\mathbf{K}'$, the surface of the second crystal is inclined by an angle β from the Bragg diffraction plane so that the surface and the diffraction plane intersect along a line parallel to $\mathbf{K}_0 + \mathbf{K}_h$.

The radiation scattered by the second crystal at position $\bar{y}$ in the direction $\mathbf{K}'$ is energy analyzed by means of a solid-state detector (detector 1 of Fig. 1). Let $A(\omega - \bar{\omega})$ be the energy resolution function of this detector, then the energy distribution $I(\bar{\omega}, \bar{y})$ of the scattered intensity is given by the following relation taking into account (3.9) together with (4.1)

$$\begin{aligned} I(\bar{\omega}, \bar{y}) = r_0^2 [(\omega_0 - \bar{\omega})/\omega_0] \tfrac{1}{2} I_0 \rho_e \int \mathrm{d}\omega \, A(\omega - \bar{\omega}) \\ \times \sum_{\nu=1}^{2} \{ F_1^{(\nu)}(\bar{y}, \bar{\omega}) \mathcal{J}_{\mathbf{q}_0,0}(\omega) \\ + F_2^{(\nu)}(\bar{y}, \bar{\omega}) \mathcal{J}_{\mathbf{q}_h,0}(\omega) \\ + F_3^{(\nu)}(\bar{y}, \bar{\omega}) [\mathcal{J}_{\mathbf{q}_0,\mathbf{g}_h}(\omega) + \mathcal{J}^*_{\mathbf{q}_h,-\mathbf{g}_h}(\omega)] \\ + F_3^{*(\nu)}(\bar{y}, \bar{\omega}) [\mathcal{J}_{\mathbf{q}_h,-\mathbf{g}_h}(\omega) + \mathcal{J}^*_{\mathbf{q}_0,\mathbf{g}_h}(\omega)], \end{aligned} \tag{4.18}$$

where ρ_e is the electron density of the sample crystal. The functions F_1, F_2, F_3 take into account both the initial photon state, which is determined by $\bar{y}$, and the weight of the different polarization states that are involved:

$$\begin{aligned} F_1^{(\nu)}(\bar{y}, \bar{\omega}) \equiv (P_0^{(\nu)})^2 \int_0^{+\infty} \int_{-\infty}^{+\infty} \exp\{-[\sigma^{(\nu)}(B y_{\mathrm{I}}^{(\nu)}) \\ + \mu(\omega_0 - \bar{\omega})/\cos\alpha] z\} \\ \times |\xi_{\mathrm{I}}^{(\nu)}(y_{\mathrm{I}}^{(\nu)} - \bar{y})|^2 \, \mathrm{d}y_{\mathrm{I}}^{(\nu)} \, \mathrm{d}z \end{aligned} \tag{4.19}$$

$$\begin{aligned} F_2^{(\nu)}(\bar{y}, \bar{\omega}) \equiv (P_h^{(\nu)})^2 \int_0^{+\infty} \int_{-\infty}^{+\infty} \exp\{-[\sigma^{(\nu)}(B y_{\mathrm{I}}^{(\nu)}) \\ + \mu(\omega_0 - \bar{\omega})/\cos\alpha] z\} \\ \times |\xi_{\mathrm{I}}^{(\nu)}(y_{\mathrm{I}}^{(\nu)} - \bar{y})|^2 \\ \times |\xi_{\mathrm{II}}^{(\nu)}(B y_{\mathrm{I}}^{(\nu)})|^2 \, \mathrm{d}y_{\mathrm{I}}^{(\nu)} \, \mathrm{d}z \end{aligned} \tag{4.20}$$

$$\begin{aligned} F_3^{(\nu)}(\bar{y}, \bar{\omega}) \equiv P_0^{(\nu)} P_h^{(\nu)} \int_0^{+\infty} \int_{-\infty}^{+\infty} \exp\{-[\sigma^{(\nu)}(B y_{\mathrm{I}}^{(\nu)}) \\ + \mu(\omega_0 - \bar{\omega})/\cos\alpha] z\} \\ \times |\xi_{\mathrm{I}}^{(\nu)}(y_{\mathrm{I}}^{(\nu)} - \bar{y})|^2 \\ \times \xi_{\mathrm{II}}^{(\nu)}(B y_{\mathrm{I}}^{(\nu)}) \, \mathrm{d}y_{\mathrm{I}}^{(\nu)} \, \mathrm{d}z, \end{aligned} \tag{4.21}$$

where $\mu(\omega_0 - \bar{\omega})$ is the linear absorption coefficient of the sample crystal for the scattered radiation of energy $\omega' = \omega_0 - \bar{\omega}$. α is the angle between $\mathbf{n}$, the surface normal of the second crystal, and $\mathbf{K}'$ (see Fig. 1). The polarization factors $P_0^{(\nu)}$ and $P_h^{(\nu)}$, respectively, are specified for the case $\mathbf{K}' \cdot \mathbf{g}_h = 0$, which is equivalent to $q_0^2 = q_h^2$:

$$P_0^{(1)} \equiv (\mathbf{e}_0 \cdot \mathbf{e}')^{(1)} = (1 - \tan^2\theta_B \cos\theta_c)^{1/2} \tag{4.22}$$

$$P_h^{(1)} \equiv (\mathbf{e}_h \cdot \mathbf{e}')^{(1)} = P_0^{(1)} \tag{4.23}$$

$$P_0^{(2)} \equiv (\mathbf{e}_0 \cdot \mathbf{e}')^{(2)} = -\cos\theta_c \tag{4.24}$$

$$P_h^{(2)} \equiv (\mathbf{e}_h \cdot \mathbf{e}')^{(2)} = P_0^{(2)}, \tag{4.25}$$

where θ_c is the scattering angle defined by

$$\cos\theta_c = \mathbf{K}_0 \cdot \mathbf{K}' / |\mathbf{K}_0||\mathbf{K}'|. \tag{4.26}$$

Assuming $\mathbf{q}_0$ and $\mathbf{q}_h$ to be equivalent with respect to crystal symmetry, and letting $q_0 = q_h = q$, then we find, in the first place, that the two Compton profiles of (4.18) are identical. In the second place, the nondiagonal profiles within the [ ] brackets of (4.18) are identical.

In this case the nondiagonal profile

$$\int \Gamma(\mathbf{p} + \mathbf{g}_h | \mathbf{p}) \delta(\omega - q^2/2m - \mathbf{p} \cdot \mathbf{q}/m) \, \mathrm{d}\mathbf{p} + \mathrm{cc} \tag{4.27}$$

[convoluted with the energy resolution function $A(\omega - \bar{\omega})$] can be obtained from measurements of the energy distribution $I(\bar{\omega}, \bar{y})$ of the scattered intensity for different values of $\bar{y}$, which means for different initial photon states (or different values of F_1, F_2 and F_3), provided that I_0 is the same for all relative angular positions of the double-crystal setting. If the 'nondiagonal profile' is real valued, at least two measurements will be necessary. The normalization of the profiles can be done easily, if one of the measurements is at a very large value of $\bar{y}$, so that $F_2 = F_3 = 0$. In this case the normalization of the measured spectrum $I(\bar{\omega}, \bar{y})$, after being transformed into a Q scale according to

$$Q \equiv \mathbf{p} \cdot \mathbf{q}/\mathbf{q} = \omega m/q - q/2, \tag{4.28}$$

is based on the following approximation as utilized in most Compton scattering studies:

$$\begin{aligned} \int_0^{Q_m} \int\int \Gamma(\mathbf{p}|\mathbf{p}) \delta(\omega - \hbar q^2/2m - Qq/m) \, \mathrm{d}\mathbf{p} \\ \times A(\omega - \bar{\omega}) \, \mathrm{d}\omega \, \mathrm{d}Q \\ \simeq \tfrac{1}{2} n_v + \int_0^{Q_m} \int\int \Gamma_{cf}(\mathbf{p}|\mathbf{p}) \, \delta(\omega - \hbar q^2/2m - Qq/m) \, \mathrm{d}\mathbf{p} \\ \times A(\omega - \bar{\omega}) \, \mathrm{d}\omega \, \mathrm{d}Q, \end{aligned} \tag{4.29}$$

where Q_m has to be chosen large enough so that the range $-Q_m < Q < Q_m$ covers the whole valence-electron Compton profile; n_v is the number of valence electrons per atom. Γ_{cf}, the core-electron part of the density matrix, is calculated by using a superposition of free-atom wave functions. Γ_{cf} is assumed to be normalized to n_c, the number of core electrons per atom, according to

$$\int \Gamma_{cf}(\mathbf{p}|\mathbf{p})\, d\mathbf{p} = n_c. \tag{4.30}$$

Let $f(\mathbf{g}_h)$ be the well known X-ray form factor, then the following sum rule (Benesch, Singh & Smith, 1971)

$$\int \Gamma(\mathbf{p}|\mathbf{p}+\mathbf{g}_h)\, d\mathbf{p} = f(\mathbf{g}_h) \tag{4.31}$$

provides additionally a good consistency test on the experimental nondiagonal profiles $\mathcal{J}_{\mathbf{q},\mathbf{g}_h}(Q)$ if appropriate experimental values of $f(g_h)$ are available.

V. Experimental details and results

The nondiagonal profiles of Si valence electrons that contain the desired information about the nondiagonal momentum density were obtained for two different reciprocal-lattice vectors, $\mathbf{g}_h = (2\pi/a)(220)$ and $\mathbf{g}_h(2\pi/a)(111)$, by measuring the DDCS's and by using the evaluation procedure as described in § IV.

1. $\mathbf{g}_{220}$ *experiment*

In the case of the $\mathbf{g}_{220}$ experiment, the first crystal of the double-crystal setting (Fig. 1) was a symmetrically cut (220) crystal. The surface of the second crystal was inclined by an angle $\beta = 15°$ from the (220) plane. The scattering angle θ_c between $\mathbf{K}_0$ and $\mathbf{K}'$ on one side and $\mathbf{K}_h$ and $\mathbf{K}'$ on the other side was 128(2)°. The tolerance ±2° is due to both the size of the irradiated area at the second crystal and the effective area of the Si(Li) detector crystal (detector 1 of Fig. 1). The orientation of $\mathbf{K}'$ relative to the sample crystal was chosen in a manner so that, in the first place, the scattering vectors $\mathbf{q}_0$ and $\mathbf{q}_h$ had equal length, in order to fulfill the demand of (3.4). In the second place, the orientation of $\mathbf{K}'$ guaranteed that the direction of $\mathbf{q}_0$ and $\mathbf{q}_h$ coincided with the direction of $\mathbf{g}_{9\bar{7}7}$ and $\mathbf{g}_{7\bar{9}7}$, respectively, in order to make them equivalent with respect to the crystal symmetry. Therefore, the reduced equation (3.5) can be used for evaluating the measurements. $K_{\alpha_{1,2}}$ X-radiation of an Mo tube was employed. The total energy resolution $A(\omega - \bar{\omega})$ of the experiment, as due to the MoK doublet and the Si(Li) detector resolution, was measured by energy analyzing the Bragg-reflected intensity using the Si(Li) detector at the position of detector 2 in Fig. 1. The double differential scattering cross section was measured for the following eight angular positions $\bar{y}$ of the second crystal relative to the first one (given in units of $y_{II}^{(1)}$): −88·4, −8·84, −1·58, −0·82, 0·82, 1·58, 2·18, 8·84. The relative angular position $\bar{y}$ of the sample crystal is read and kept constant to 0.2″ by computer feedback through the rocking-curve intensity measured by detector 2.

The spectrum of the scattered radiation contained $\sim 3{\cdot}5 \times 10^5$ counts in every case after a linear background subtraction. The (quasi)-elastically scattered part of the spectrum was fitted at its high-energy side on the total energy resolution function and then subtracted from the spectrum in order to isolate the inelastic part.

Then the energy scale was converted into a Q scale according to (4.38). Only the scattered spectrum between $Q = 0$ and $Q = 2{\cdot}5$ a.u. (high-energy side) is used to extract the valence-electron nondiagonal profile according to the procedure described in § IV, since the low-energy part of the spectrum is contaminated by the inset of the $1s^2$ part of the profiles as due to the binding energy of the Si K electrons. The spectra were normalized in the manner as described

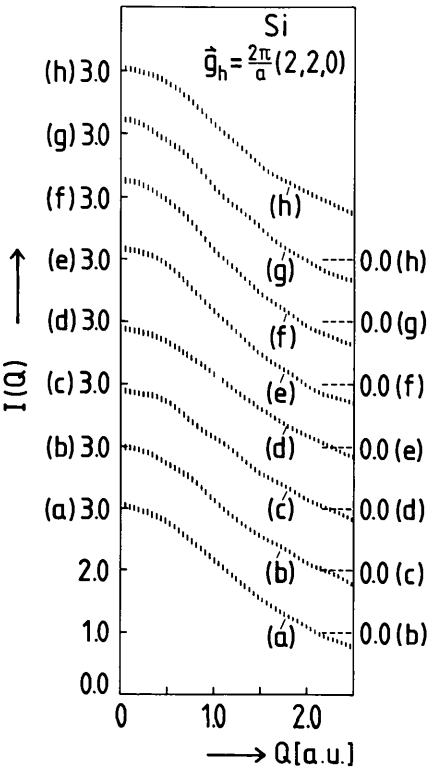

Fig. 2. Normalized high-energy part of the Si 220 spectra after subtraction of both a linear background and the (quasi) elastically scattered line for eight different values of $\bar{y}$, the relative angular position of the second crystal with respect to the first. The curves refer to the following values of $\bar{y}$ in units of $y_{II}^{(1)}$: (*a*) −88·4; (*b*) −8·84; (*c*) −1·58; (*d*) −0·82; (*e*) +0·82; (*f*) +1.58; (*g*) +2·18; (*h*) +8·84. The statistical error of each measured point is represented by the length of the streak. The curves were smoothed with an appropriate digital filter. The energy scale of the measurement was converted into a Q scale. Different contributions of nondiagonal profiles to the spectra for different $\bar{y}$ are evident.

in § IV [(4.29)] by utilizing the measurement with $y=-88{\cdot}4$. The Compton profile of the $2s^22p^6$ core electrons on the right-hand side of (4.29) was calculated by using Clementi (1965) wave functions. This profile was convoluted with a Gaussian of 1·72 a.u. full width at half maximum (FWHM) on the Q scale, which is composed of the total energy resolution of the experiment (after being converted into a Q scale) and the influence of a Gaussian-distributed scattering angle θ_c.

The normalized high-energy part of the spectra for eight values of $\bar{y}$ are displayed in Fig. 2. The different shape of the spectra, as can be read, for instance, from different intensity at $Q=0$, is due to different contributions of the nondiagonal profiles.

By using in each case a pair of measured spectra belonging to two different values of $\bar{y}$, the spectra could be separated into their Compton profile and their nondiagonal profile contribution according to (4.18). In order to do this, the factors $F_1^{(\nu)}$, $F_2^{(\nu)}$, $F_3^{(\nu)}$ were calculated according to (4.19)–(4.21) assuming unpolarized radiation hitting the first crystal and using both the well known relation between χ_{rh} and the structure factor F_h and the correspondence between χ_{i0} and μ, the linear absorption coefficient. $\chi_{i(220)}$ is assumed to be $0{\cdot}96\times\chi_{i0}$ (Hildebrandt, Stephenson & Wagenfeld, 1973).

Finally, the core contribution to the 220 nondiagonal profiles was calculated by using Clementi wave functions together with the relations as derived in Appendix *C*. These core contributions were subtracted from the total 220 nondiagonal profiles, thus obtaining the interesting valence-electron (220) nondiagonal profiles. A weighted average of all valence-electron 220 nondiagonal profiles, as obtained by evaluating the measured spectra in pairs, is shown in Fig. 3, together with the corresponding valence-electron Compton profile. This Compton profile is also the result of an evaluation of the measured spectra in pairs, where, in each case, the core contribution was also subtracted from the total Compton profile. Together with the experimental profiles in Fig. 3, their theoretical free-atom $3s^23p^2$ and $3s^13p^3$ counterparts are also displayed, which were obtained from Clementi wave functions and convoluted with a Gaussian of FWHM = 1·72 a.u. According to (1) the integration of the experimental 220 nondiagonal profiles over the whole Q scale should yield the $f(\mathbf{g}_{220})$ X-ray form factor of Si valence electrons. If the small asymmetry with respect to $Q=0$ is neglected, which is always present in a nondiagonal profile due to

$$\Gamma(\mathbf{p}+\mathbf{g}_h|\mathbf{p})=\Gamma(\tilde{\mathbf{p}}+\mathbf{g}_h|\tilde{\mathbf{p}}), \tag{5.1}$$

where

$$\tilde{\mathbf{p}}\equiv-(\mathbf{p}+\mathbf{g}_h), \tag{5.2}$$

integration of the 220 nondiagonal profile over Q from 0 to $+Q_m$ [see (4.29)] should yield $\frac{1}{2}f(\mathbf{g}_{220})$.

The corresponding integral of the experimental valence-electron 220 nondiagonal profile over Q from $Q=0$ to $Q=2{\cdot}5$ a.u. is 0.00(2). The best experimental value of $\frac{1}{2}f(\mathbf{g}_{220})$ for valence electrons is −0.02 obtained by subtracting $f_{Si^{4+}}(\mathbf{g}_{220})=8{\cdot}694$ (see *International Tables for X-ray Crystallography*, 1968) from the measured value of the total form factor $f_{Si}(\mathbf{g}_{220})=8{\cdot}651$ (Aldred & Hart, 1973). This agreement between the integrated nondiagonal profile with the corresponding experimental X-ray form factor can be considered as a successful test on the reliability of the measured nondiagonal profiles.

2. $\mathbf{g}_{111}$ *experiment*

In the case of the $\mathbf{g}_{111}$ experiment, the first crystal of the double-crystal setting (Fig. 2) was an asymmetrically cut crystal with an angle $\varphi=5°$ between the surface and the (111) plane. The scattering angle θ_c was 130(2)°. The orientation of $\mathbf{K}'$ again was chosen to make possible both equal length of the scattering vectors $\mathbf{q}_0$ and $\mathbf{q}_h$ and equivalence of $\mathbf{q}_0$ and $\mathbf{q}_h$ with respect to the crystal symmetry, where their directions were those of $\mathbf{g}_{20,\bar{1}8,1}$ and $\mathbf{g}_{18,\bar{2}0,\bar{1}}$, respectively. Again,

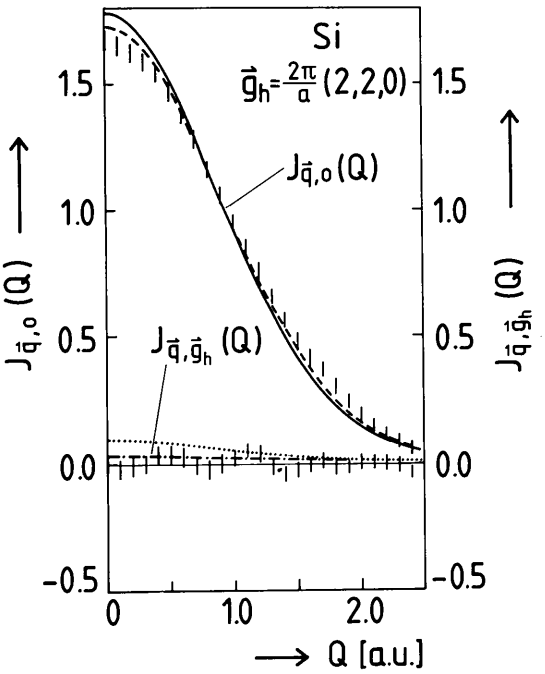

Fig. 3. Upper curves: Experimental Si valence-electron Compton profile $\mathcal{J}_{\mathbf{q},0}(Q)$ [$\mathbf{q}\|(9\bar{7}7)$], together with a free-atom $3s^23p^2$ Compton profile (solid line) and a free-atom $3s^13p^3$ Compton profile (dashed line) both convoluted with a Gaussian of FWHM = 1·72 a.u. (total momentum-space resolution of the experiment). The length of the streaks in the experimental curve represents statistical error. Lower curves: Experimental Si valence-electron 220 nondiagonal profile $\mathcal{J}_{\mathbf{q},\mathbf{g}_{220}}(Q)$ [$\mathbf{q}\|(9\bar{7}7)$], together with a free-atom $3s^23p^2$ 220 nondiagonal profile (dotted line) and a free-atom $3s^13p^3$ 220 nondiagonal profile (dashed-dotted line), both convoluted with a Gaussian of FWHM = 1·72 a.u.

$K_{\alpha_{1,2}}$ radiation of an Mo tube was used. The angle β (see Fig. 1) between the (111) plane and the surface of the second (sample) crystal was 4·5°. The total energy resolution $A(\omega-\bar{\omega})$ was the same as in the $\mathbf{g}_{220}$ experiment. Three spectra were measured at the following angular positions $\bar{y}$ of the second crystal in units of $y_{II}^{(1)}$: −64·8, −1·31, +1·31. The spectrum of the scattered radiation contained $\sim 7{\cdot}5\times10^5$ counts in every case after background subtraction. Normalization and conversion of the energy scale into the Q scale was done as in the g_{220} case. In Fig. 4 the normalized high-energy parts of the spectra for three $\bar{y}$ values are shown. Again the different contributions of the nondiagonal profiles to the total spectra are evident.

The extraction of the valence-electron 111 nondiagonal profiles was performed in the same manner as in the $\mathbf{g}_{220}$ case. In Fig. 5 the experimental valence-electron 111 nondiagonal profile is shown together with the experimental valence-electron Compton profile. The theoretical free-atom counterparts of the experimental profiles are also displayed (again convoluted with a Gaussian of FWHM = 1·72 a.u.).

The integral of the experimental valence-electron 111 nondiagonal profile over Q from $Q=0$ to $Q=$ 2·5 a.u. is 0·65(2). The corresponding experimental value of half the X-ray form factor, $\frac{1}{2}f(\mathbf{g}_{111})$, is 0·632 (Aldred & Hart, 1973), so that in the $\mathbf{g}_{111}$ case the measured nondiagonal profile also seems to be quite reliable.

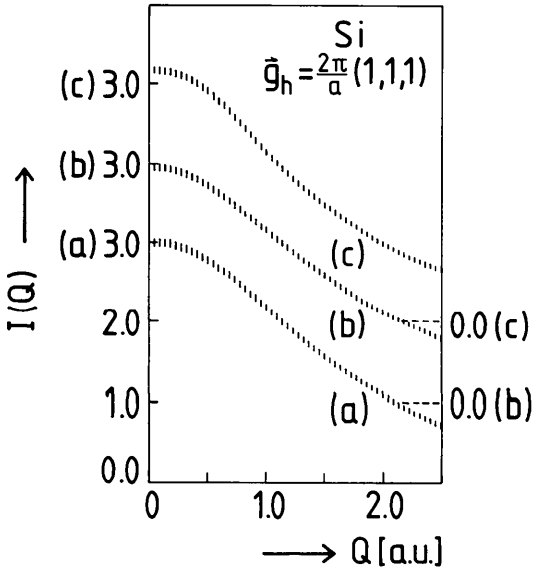

Fig. 4. Normalized high-energy part of the Si 111 spectra after subtraction of both the background and the (quasi) elastically scattered line for the following three values of $\bar{y}$ (in units of $y_{II}^{(1)}$): (*a*) −64·8; (*b*) −1·31; (*c*) +1·31. Representation of statistical error as in Fig. 2. Different contributions of nondiagonal profiles to the spectra for different $\bar{y}$ are evident.

VI. Discussion

One should bear in mind that the experimental results presented here are only of a very preliminary nature. The poor energy resolution and the low statistical accuracy together with the limitation to only one projection prevent detailed experimental information about the *three-dimensional* nondiagonal momentum density. Nevertheless, some general features of the solid-state Si nondiagonal momentum density can be deduced.

The much higher sensitivity of the nondiagonal density to solid-state effects is demonstrated very clearly by the 111 results: The difference between the free-atom Compton profile and the experimental one is less than 3% at $Q=0$, when the $3s^13p^3$ atomic configuration is taken into account. On the contrary, this difference is more than 20% in the case of the nondiagonal profiles; moreover, this difference has the opposite sign. This reflects the special phase relationship between $\chi(\mathbf{p})$ and $\chi^*(\mathbf{p}+\mathbf{g}_h)$, the momentum-space wavefunctions at $\mathbf{p}$ and $\mathbf{p}+\mathbf{g}_h$, in the case of a solid when compared with free-atom states. In particular, it is the role of the higher momentum expansion coefficients of the real-space wave function brought about by the lattice periodicity of

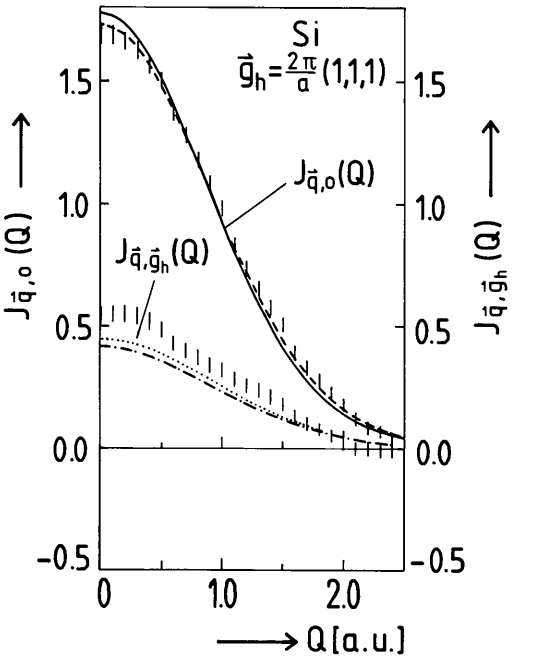

Fig. 5. Upper curves: Experimental Si valence-electron Compton profile $J_{\mathbf{q},o}(Q)$ [$\mathbf{q}\|(20,\overline{1}8,1)$], together with a free-atom $3s^23p^2$ Compton profile (solid line) and a free-atom $3s^13p^3$ Compton profile (dashed line) both convoluted with a Gaussian of FWHM = 1·72 a.u. (total momentum-space resolution). Statistical error is given by the length of the streaks representing measuring points. Lower curves: Experimental Si valence-electron 111 non-diagonal profile $J_{\mathbf{q},\mathbf{g}_{111}}(Q)$ [$\mathbf{q}\|(20,\overline{1}8,1)$], together with a free-atom $3s^23p^2$ 111 nondiagonal profile (dotted line), and a free-atom $3s^13p^3$ 111 nondiagonal profile (dashed-dotted line) both convoluted with a Gaussian of FWHM = 1·72 a.u.

the ion potential (Berko & Plaskett, 1958) that makes the nondiagonal momentum-space density much more sensitive to solid-state effects than the diagonal density. This can be made evident for a simple solid with only one occupied band in the ground state:

Let the real-space wave function $\psi_{\mathbf{k}}(\mathbf{r})$ ($\mathbf{k}$ = Bloch-wave vector) of this model solid be expanded into plane waves according to

$$\psi_{\mathbf{k}}(\mathbf{r}) = \sum_{g_h} a(\mathbf{k}+\mathbf{g}_h) \exp[i(\mathbf{k}+\mathbf{g}_h)\mathbf{r}]. \qquad (6.1)$$

Then the expansion coefficient $a(\mathbf{k}+\mathbf{g}_h)$ with $\mathbf{g}_h \neq \mathbf{0}$ may be called the higher momentum coefficient, since $|a(\mathbf{k}+\mathbf{g}_h)|^2$ is the probability for measuring a momentum $\mathbf{p} = \hbar(\mathbf{k}+\mathbf{g}_h)$, a so-called higher momentum component of the momentum probability distribution. The coefficient $a(\mathbf{k}+\mathbf{0})$ is called the fundamental.

The nondiagonal density corresponding to any $\mathbf{g}_h$ couples the $\mathbf{g}_h$th higher momentum coefficient with the fundamental. Therefore, the contribution of higher momentum coefficients to the nondiagonal momentum density is augmented by the magnitude of the fundamental coefficient, whereas the higher momentum coefficients contribute to the diagonal momentum density only *via* its squared modulus.

This emphasis of higher momentum coefficients is also visible in the 220 results: Since, in the case of Si, all occupied states are restricted to the so-called Jones zone (Jones, 1975), the 220 nondiagonal density exclusively couples fundamentals with higher momentum coefficients also in the case of a solid with four occupied bands. Therefore, one can easily understand why, compared to the free-atom case, the 220 nondiagonal profile is smaller and, at least for certain Q ranges, opposite in sign, reflecting the opposite sign of the higher momentum coefficients compared with their corresponding fundamentals in most cases.

In order to improve the experimental information about the nondiagonal momentum density by means of coherent Compton scattering, one has to follow two lines: First of all the momentum-space resolution has to be improved by replacing the energy-dispersive analysis by a crystal-dispersive one (Schülke & Nagasawa, 1984). Additionally, a higher statistical accuracy has to be achieved. Both can be done by utilizing the potentiality of a powerful synchrotron source. In this case, X-ray band-pass filters (Schülke, Mourikis & Liedtke, 1984) could also be employed. In the second place, nondiagonal profiles with many different directions of the scattering vectors have to be measured, in order to render the application of one of the well known reconstruction methods that yield the three-dimensional nondiagonal momentum density.

Helpful discussions with U. Bonse are kindly acknowledged. We thank the Deutsche Forschungsgemeinschaft for financial support.

APPENDIX *A*

As an example for the formalism of the impulse approximation as applied to the double differential cross section of coherent inelastic scattering, the approximated expression of the following cross term in the [ ] brackets of (2.16) should be derived:

$$\rho^*_{\mathbf{q}_0,f,i}\rho_{\mathbf{q}_h,f,i}\delta(E_f - E_i - \hbar\omega) \equiv \sum_f \langle i|e^{-i\mathbf{q}_0\cdot\mathbf{r}}|f\rangle\langle f|e^{i\mathbf{q}_h\cdot\mathbf{r}}|i\rangle\delta(E_f - E_i - \hbar\omega), \qquad (A.1)$$

where $|i\rangle$ and $|f\rangle$ stand for the initial and final states of the scattering system, respectively. For the sake of simplicity, this sytem is thought of as a one-electron system by skipping the j summation in (2.14), (2.16). The extension to many-particle systems is given in Appendix *B*. The following derivation follows very closely the formalism as applied by Eisenberger & Platzman (1970) to the conventional inelastic scattering.

By using the integral representation of the δ function, one obtains for (*A*.1)

$$\tfrac{1}{2}\Big\{\sum_f \int_{-\infty}^{+\infty} dt\, e^{-i\omega t}\langle i|\, e^{-i\mathbf{q}_0\cdot\mathbf{r}}|f\rangle\langle f|\, e^{iE_f t/\hbar}\, e^{i\mathbf{q}_h\cdot\mathbf{r}}\, e^{-iE_i t/\hbar}|i\rangle + \int_{-\infty}^{+\infty} e^{i\omega t}\,\langle i|\, e^{iE_i t/\hbar}\, e^{-i\mathbf{q}_0\cdot\mathbf{r}}\, e^{-iE_f t/\hbar}|f\rangle\langle f|e^{i\mathbf{q}_h\cdot\mathbf{r}}|i\rangle\Big\}. \qquad (A.2)$$

This representation was chosen in order to keep the cross term of (2.16) real valued throughout the following approximation procedure.

$$H = (2m)^{-1}p^2 + V \equiv H_0 + V \qquad (A.3)$$

is the Hamiltonian of the scattering system, (*A*.2) will read as follows:

$$\tfrac{1}{2}\Big\{\int_{-\infty}^{+\infty} dt\, e^{-i\omega t}\langle i|e^{-i\mathbf{q}_0\mathbf{r}}\, e^{iHt/\hbar}\, e^{i\mathbf{q}_h\cdot\mathbf{r}}\, e^{-iHt/\hbar}|i\rangle + \int_{-\infty}^{+\infty} dt\, e^{i\omega t}\langle i|e^{iHt/\hbar}\, e^{-i\mathbf{q}_0\cdot\mathbf{r}}\, e^{-iHt/\hbar}\, e^{i\mathbf{q}_h\cdot\mathbf{r}}|i\rangle\Big\}, \qquad (A.4)$$

where additionally the completeness relation

$$\sum_f |f\rangle\langle f| = 1 \qquad (A.5)$$

was used.

If $e^{iHt/\hbar}$ is expanded in the following manner

$$e^{iHt/\hbar} = e^{iH_0 t/\hbar}\, e^{iVt/\hbar}\, e^{-\frac{1}{2}[H_0, V]t^2/\hbar}\ldots, \qquad (A.6)$$

the essential of the impulse approximation consists of the assumption that

$$\exp(-\tfrac{1}{2}[H_0, V]t^2/\hbar^2) \simeq 1, \qquad (A.7)$$

which is justified when

$$\hbar\omega \gg \langle[H_0, V]\rangle^{1/2}, \qquad (A.8)$$

since appreciable contributions to the integrals in

(A.4) occur only for $t \lesssim 1/\omega$. The relation (A.8) will be valid if the transferred energy $\hbar\omega$ is large compared with characteristic energies of the system.

Equation (A.7) together with $[V_1\mathbf{r}]=0$ results in

$$\tfrac{1}{2}\Big\{\int_{-\infty}^{+\infty} dt\, e^{-i\omega t}\langle i|\, e^{-i\mathbf{q}_0\cdot\mathbf{r}}\, e^{iH_0 t/\hbar}\, e^{i\mathbf{q}_h\cdot\mathbf{r}}\, e^{-iH_0 t/\hbar}|i\rangle + \int_{-\infty}^{+\infty} dt\, e^{i\omega t}\langle i|\, e^{iH_0 t/\hbar}\, e^{-i\mathbf{q}_0\cdot\mathbf{r}}\, e^{-iH_0 t/\hbar}\, e^{i\mathbf{q}_h\cdot\mathbf{r}}|i\rangle\Big\} \quad (A.9)$$

for (A.4).

Finally, the insertion of a complete system of eigenfunctions $|\mathbf{p}\rangle$ of H_0, together with

$$e^{iH_0 t/\hbar}|p\rangle = e^{i\varepsilon_{\mathbf{p}} t/\hbar}|p\rangle,$$

where

$$\varepsilon_{\mathbf{p}} \equiv \mathbf{p}^2/2m, \quad (A.10)$$

transforms (A.9) into

$$\tfrac{1}{2}\Big\{\sum_{\mathbf{p}}\langle i|\mathbf{p}-\mathbf{q}_0\rangle\langle\mathbf{p}-\mathbf{q}_h|i\rangle\delta(\varepsilon_{\mathbf{p}}-\varepsilon_{\mathbf{p}-\mathbf{q}_h}-\hbar\omega) + \sum_{\mathbf{p}}\langle i|\mathbf{p}-\mathbf{q}_0\rangle\langle\mathbf{p}-\mathbf{q}_h|i\rangle\delta(\varepsilon_{\mathbf{p}}-\varepsilon_{\mathbf{p}-\mathbf{q}_0}-\hbar\omega)\Big\}, \quad (A.11)$$

where the integral representation of the δ function was revoked.

By means of the substitutions $\mathbf{p}-\mathbf{q}_h=\mathbf{p}_0$ in the first and $\mathbf{p}-\mathbf{q}_0=\mathbf{p}_0$ in the second terms of (A.11), and by taking into account that $\mathbf{q}_0=\mathbf{q}_h+\mathbf{g}_h$, according to (2.14), one ends up with

$$\tfrac{1}{2}\Big\{\sum_{\mathbf{p}_0}\langle i|\mathbf{p}_0-\mathbf{g}_h\rangle\langle\mathbf{p}_0|i\rangle\delta(\omega-\hbar q_h^2/2m-\mathbf{p}_0\cdot\mathbf{q}_h/m + \sum_{\mathbf{p}_0}\langle i|\mathbf{p}_0\rangle\langle\mathbf{p}_0+\mathbf{g}_h|i\rangle\delta(\omega-\hbar q_0^2/2m-\mathbf{p}_0\cdot\mathbf{q}_0/m)\Big\} \quad (A.12)$$

instead of (A.11).

In the same manner the impulse approximation of (2.16) can be achieved so that (3.2) is obtained.

APPENDIX B

The impulse approximation of (2.16) is now extended to many-particle systems. Again, only the impulse approximation of *one* cross term in the [ ] brackets of (2.16) should be derived explicitly, namely

$$\left\langle f\left|\sum_j e^{i\mathbf{q}_0\cdot\mathbf{r}_j}\right|f\right\rangle\left\langle i\left|\sum_j e^{-i\mathbf{q}_h\cdot\mathbf{r}_j}\right|f\right\rangle\delta(E_f-E_i=\hbar\omega). \quad (B.1)$$

With the same argument as used in Appendix A, (B.1) can be represented by

$$\tfrac{1}{2}\Big\{\int_{-\infty}^{+\infty} dt\, e^{-i\omega t}\sum_{jk}\langle i|e^{-i\mathbf{q}_h\cdot\mathbf{r}_j}\, e^{iH_0 t/\hbar}\, e^{i\mathbf{q}_0\cdot\mathbf{r}_k}\, e^{-iH_0 t/\hbar}|i\rangle + \int_{-\infty}^{+\infty} dt\, e^{i\omega t}\sum_{jk}\langle i|e^{iH_0 t/\hbar}\, e^{-i\mathbf{q}_h\cdot\mathbf{r}_j}\, e^{-iH_0 t/\hbar}\, e^{i\mathbf{q}_0\cdot\mathbf{r}_k}|i\rangle\Big\}, \quad (B.2)$$

with

$$\hbar\omega \gg \langle[H_0, V]\rangle^{1/2}. \quad (B.3)$$

Further detailed derivation will refer only to the first term of (B.2).

In order to introduce the (spin-free) one- and two-particle density matrices according to Löwdin's (1956) convention, the first term of (B.2) has to be separated into one- and two-particle contributions:

$$\int_{-\infty}^{+\infty} dt\, e^{-i\omega t}\{N\langle i|\, e^{-i\mathbf{q}h\cdot\mathbf{r}_1}\, e^{iH_0 t/\hbar}\, e^{i\mathbf{q}_0\cdot\mathbf{r}_1}\, e^{-H_0 t/\hbar}|i\rangle + 2\tbinom{N}{2}\langle i|\, e^{-i\mathbf{q}_h\cdot\mathbf{r}_1}\, e^{iH_0 t/\hbar}\, e^{i\mathbf{q}_0\cdot\mathbf{r}_2}\, e^{-iH_0 t/\hbar}|i\rangle\}. \quad (B.4)$$

By writing (B.4) in terms of the one-particle density matrix $\Gamma_1(\mathbf{r}|\mathbf{r}')$ and the two-particle density matrix $\Gamma_2(\mathbf{r}_1\mathbf{r}_2|\mathbf{r}_1'\mathbf{r}_2')$, respectively, one obtains

$$\int_{-\infty}^{+\infty} dt\, e^{-i\omega t}\{N\int e^{-i\mathbf{q}_h\cdot\mathbf{r}_1} \times e^{iH_0 t/\hbar}\, e^{i\mathbf{q}_0\cdot\mathbf{r}_1}\, e^{-iH_0 t/\hbar}\Gamma_1(\mathbf{r}_1|\mathbf{r}_1')\, d\mathbf{r}_1 \times 2\tbinom{N}{2}\int e^{-i\mathbf{q}_h\cdot\mathbf{r}_1}\, e^{iH_0 t/\hbar}\, e^{i\mathbf{q}_0\cdot\mathbf{r}_2} \times e^{-iH_0 t/\hbar}\Gamma_2(\mathbf{r}_1\mathbf{r}_2|\mathbf{r}_1'\mathbf{r}_2')\, d\mathbf{r}_1\, d\mathbf{r}_2\}. \quad (B.5)$$

As in the case of the approximation procedure, described in Appendix A, one inserts into (B.5) a complete system of eigenfunctions $|\mathbf{p}\rangle$ of H_0 so that one obtains

$$\int_{-\infty}^{+\infty} dt\,\{e^{-i(\hbar\omega-\varepsilon_{\mathbf{p}}+\varepsilon_{\mathbf{p}-\mathbf{q}_0})t/\hbar}\sum_{\mathbf{p}}\int e^{i(\mathbf{p}-\mathbf{q}_h)\cdot\mathbf{r}_1} \times e^{-i(\mathbf{p}-\mathbf{q}_0)\cdot\mathbf{r}_1'}\Gamma_1(\mathbf{r}_1|\mathbf{r}_1')\, d\mathbf{r}_1\, d\mathbf{r}_1' + e^{-i(\hbar\omega-\varepsilon_{\mathbf{p}_1}-\varepsilon_{\mathbf{p}_2}+\varepsilon_{\mathbf{p}_1}+\varepsilon_{\mathbf{p}_2-\mathbf{q}_0})t/\hbar} \times \sum_{\mathbf{p}_1\mathbf{p}_2} e^{i[(\mathbf{p}_1-\mathbf{q}_h)\cdot\mathbf{r}_1+\mathbf{p}_2\cdot\mathbf{r}_2]}\, e^{-i[\mathbf{p}_1\cdot\mathbf{r}_2'+(\mathbf{p}_2-\mathbf{q}_0)\cdot\mathbf{r}_2']} \times\Gamma_2(\mathbf{r}_1\mathbf{r}_2|\mathbf{r}_1'\mathbf{r}_2')\, d\mathbf{r}_1\, d\mathbf{r}_2\, d\mathbf{r}_1'\, d\mathbf{r}_2'\}. \quad (B.6)$$

Following Benesch, Singh & Smith (1971), the n-particle density matrix in momentum space $\Gamma_n(\mathbf{p}_1\ldots\mathbf{p}_n|\mathbf{p}_1'\ldots\mathbf{p}_n')$ is defined as the $6n$-dimensional Fourier transform of the (spin-free) n-particle density matrix in position space so that (B.6) can be written as

$$\int\Gamma_1(\mathbf{p}_0+\mathbf{g}_h|\mathbf{p}_0)\delta(\omega-\hbar q_0^2/2m-\mathbf{p}_0\cdot\mathbf{q}_0/m)\, d\mathbf{p}_0 + \int\Gamma_2(\mathbf{p}_{02}-\mathbf{q}_h, \mathbf{p}_{01}+\mathbf{q}_0|\mathbf{p}_{02}, \mathbf{p}_{01}) \times\delta(\omega-\hbar q_0^2/2m-\mathbf{p}_{01}\cdot\mathbf{q}_0/m), \quad (B.7)$$

where the following substutions have been performed:

$$\mathbf{p}-\mathbf{q}_0=\mathbf{p}_0 \qquad \mathbf{p}_2-\mathbf{q}_0=\mathbf{p}_{01} \qquad \mathbf{p}_1=\mathbf{p}_{02}. \quad (B.8)$$

Additionally, the integral representation of the δ function in (B.6) was revoked.

Using the same formalism also for the second term of (*B*.2), one ends up with the following impulse approximation of (*B*.1):

$$\tfrac{1}{2}\{\int \Gamma_1(\mathbf{p}_0+\mathbf{g}_h|\mathbf{p}_0)\delta(\omega-\hbar q_0^2/2m-\mathbf{p}_0\cdot\mathbf{q}_0/m)\,d\mathbf{p}_0$$
$$+\int \Gamma_2(\mathbf{p}_{02}-\mathbf{q}_h,\mathbf{p}_{01}+\mathbf{q}_0|\mathbf{p}_{02},\mathbf{p}_{01})$$
$$\times\delta(\omega-\hbar q_0^2/2m-\mathbf{p}_{01}\cdot\mathbf{q}_0/m)\,d\mathbf{p}_{01}\,d\mathbf{p}_{02}$$
$$+\int \Gamma_1(\mathbf{p}_0|\mathbf{p}_0-\mathbf{g}_h)\delta(\omega-\hbar q_h^2/2m-\mathbf{p}_0\cdot\mathbf{q}_h/m)\,d\mathbf{p}_0$$
$$+\int \Gamma_2(\mathbf{p}_{02},\mathbf{p}_{01}|\mathbf{p}_{02}+\mathbf{q}_h,\mathbf{p}_{01}-\mathbf{q}_0)$$
$$\times\delta(\omega-\hbar q_h^2/2m-\mathbf{p}_{02}\cdot\mathbf{q}_h/m)\,d\mathbf{p}_{01}\,d\mathbf{p}_{02}\}. \qquad (B.9)$$

APPENDIX *C*

Within the limits of the one-electron approximation, $\Gamma_{cf}(\mathbf{p}|\mathbf{p}+\mathbf{g}_h)$, the $\mathbf{g}_h$th nondiagonal element of the core-electron part of the one-particle density matrix in momentum space, will be calculated for a crystal composed of free-atom cores at the positions $\mathbf{R}+\mathbf{d}_s$, where $\mathbf{R}$ is a Bravais-lattice vector and $\mathbf{d}_s$ a vector of the basis. The Bloch function of one core state may be represented in terms of the tight binding approximation by

$$\psi^s_{\mathbf{k},\nu}=V^{-1/2}\sum_{\mathbf{R}} e^{i\mathbf{k}.(\mathbf{R}+\mathbf{d}_s)}\varphi_\nu(\mathbf{r}-\mathbf{R}-\mathbf{d}_s), \qquad (C.1)$$

where φ_ν is the νth-core state of an isolated atom.

Therefore,

$$\Gamma(\mathbf{p}|\mathbf{p}+\mathbf{g}_h)=V^{-1}\sum_\nu\sum_{\mathbf{k}}\sum_s\int\sum_{\mathbf{R}} e^{-i\mathbf{k}.(\mathbf{R}+\mathbf{d}_s)}\,e^{i(\mathbf{p}+\mathbf{g}_h).\mathbf{r}}$$
$$\times\varphi^*_\nu(\mathbf{r}-\mathbf{R}-\mathbf{d}_s)\,d\mathbf{r}$$
$$\times\int\sum_{\mathbf{R}} e^{i\mathbf{k}.(\mathbf{R}+\mathbf{d}_s)}\,e^{-i\mathbf{p}.\mathbf{r}}$$
$$\times\varphi_\nu(\mathbf{r}-\mathbf{R}-\mathbf{d}_s)\,d\mathbf{r}. \qquad (C.2)$$

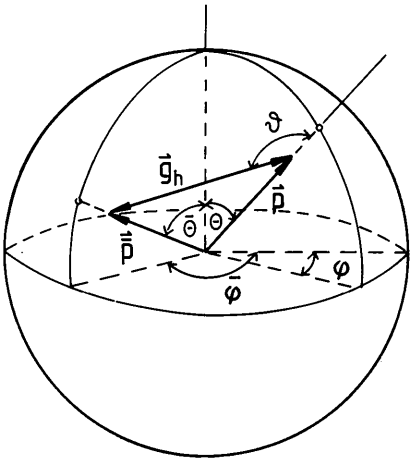

Fig. 6. Angular variables of $\mathbf{p}$ and $\bar{\mathbf{p}}\equiv\mathbf{p}+\mathbf{g}_h$ as defined in order to calculate the orientation average of the nondiagonal momentum density using free-atom wave functions.

The substitution $\mathbf{u}=\mathbf{r}-\mathbf{R}-\mathbf{d}_s$ in (*C*.2) results in

$$\Gamma(\mathbf{p}|\mathbf{p}+\mathbf{g}_h)=V^{-1}\sum_\nu\sum_{\mathbf{k}}\sum_s\{\sum_{\mathbf{R}} e^{-i(\mathbf{k}-\mathbf{p}-\mathbf{g}_h).\mathbf{R}}\,e^{-i(\mathbf{k}-\mathbf{p}-\mathbf{g}_h).\mathbf{d}_s}$$
$$\times\int\varphi^*_\nu(\mathbf{u})\,e^{i(\mathbf{p}+\mathbf{g}_h).\mathbf{u}}\,d\mathbf{u}$$
$$\times\sum_{\mathbf{R}} e^{i(\mathbf{k}-\mathbf{p}).\mathbf{R}}\,e^{i(\mathbf{k}-\mathbf{p}).\mathbf{d}_s}$$
$$\times\int\varphi_\nu(\mathbf{u})\,e^{-i\mathbf{p}.\mathbf{u}}\,d\mathbf{u}\}$$
$$=\sum_\nu\sum_{\mathbf{k}}\sum_s\{\sum_{\mathbf{g}}\delta(-\mathbf{k}+\mathbf{p}+\mathbf{g}_h-\mathbf{g})\,e^{-i(\mathbf{k}-\mathbf{p}-\mathbf{g}_h).\mathbf{d}_s}$$
$$\times\int\varphi^*_\nu(\mathbf{u})\,e^{i(\mathbf{p}+\mathbf{g}_h).\mathbf{u}}\,d\mathbf{u}$$
$$\times\sum_{\mathbf{g}}\delta(\mathbf{k}-\mathbf{p}-\mathbf{g})\,e^{i(\mathbf{k}-\mathbf{p}).\mathbf{d}_s}$$
$$\times\int\varphi_\nu(\mathbf{u})\,e^{-i\mathbf{p}.\mathbf{u}}\,d\mathbf{u}\}. \qquad (C.3)$$

Since for a given $\mathbf{p}+\mathbf{g}_h$ there exists only one $\mathbf{g}$ so that $\mathbf{p}+\mathbf{g}_h-\mathbf{g}$ is a vector within the first Brillouin zone, one ends up with

$$\Gamma(\mathbf{p}|\mathbf{p}+\mathbf{g}_h)=\sum_\nu\sum_s e^{i\mathbf{g}_h.\mathbf{d}_s}\int\varphi^*_\nu(\mathbf{u})\,e^{i(\mathbf{p}+\mathbf{g}_h).\mathbf{u}}$$
$$\times\int\varphi_\nu(\mathbf{u})\,e^{-i\mathbf{p}.\mathbf{u}}\,d\mathbf{u}$$
$$=\sum_\nu\sum_s e^{i\mathbf{g}_h.\mathbf{d}_s}\chi_\nu(\mathbf{p}+\mathbf{g}_h)\chi^*_\nu(\mathbf{p}), \qquad (C.4)$$

where $\chi_\nu(\mathbf{p})$ denotes the momentum-space wave function corresponding to the core state $\varphi_\nu(\mathbf{r})$.

Assuming the atomic cores to be completely free, one has to calculate the orientation average $F_{\nu g_h}(p,\theta)$ of $\chi_\nu(\mathbf{p}+\mathbf{g}_h)\chi^*_\nu(\mathbf{p})$, which can be written explicitly as follows

$$F_{\nu g_h}(p,\theta)=(4\pi)^{-1}\int_0^{2\pi}\int_0^{\pi}\chi^*_\nu(p,\Theta,\Phi)$$
$$\times\chi_\nu[\bar{p}(\theta),\bar{\Theta}(\theta,\Theta,\Phi),\bar{\Phi}(\theta,\Theta,\Phi)]$$
$$\times\sin\Theta\,d\Phi\,d\Phi, \qquad (C.5)$$

where

$$\cos\theta\equiv\mathbf{p}\cdot\mathbf{g}_h/pg_h \quad\text{and}\quad \bar{\mathbf{p}}\equiv\mathbf{p}+\mathbf{g}_h. \qquad (C.6)$$

Θ and Φ are the angular variables of $\mathbf{p}$. $\bar{\Theta}$ and $\bar{\Phi}$ are the angular variables of $\bar{\mathbf{p}}$ with respect to the same axis as Θ and Φ (see Fig. 6).

As indicated by (*C*.5), the orientation average of the g_hth nondiagonal matrix element of the momentum-space density exhibits cylindrical symmetry with respect to $\mathbf{g}_h$.

References

ALDRED, P. J. E. & HART, M. (1973). *Proc. R. Soc. London Ser. A*, **332**, 223–238.

BENESCH, R., SINGH, S. R. & SMITH, V. H. JR (1971). *Chem. Phys. Lett.* **10**, 151–153.

BENESCH, R. & SMITH, V. H. JR (1973). *Wave Mechanics - The First Fifty Years*, edited by W. C. PRICÉ, S. S. CHISSIK & T. RAVENSDALE, pp. 203–209. London: Butterworths.

BERKO, S. & PLASKETT, J. S. (1958). *Phys. Rev.* **112**, 1877–1887.

BONSE, U. (1964). *Z. Phys.* **177**, 385-423.
CHANG, S. L. & HAN, F.-S. (1982). *Acta Cryst.* A**38**, 414-417.
CLEMENTI, E. (1965). *IBM J. Res. Dev.* **9**, 2-92.
EISENBERGER, P. & PLATZMAN, P. M. (1970). *Phys. Rev. A*, **2**, 415-423.
GOLOVCHENKO, J. A., KAPLAN, D. R., KINCAID, B., LEVESQUE, R., MEIXNER, A., ROBBINS, M. P. & FELSTEINER, J. (1981). *Phys. Rev. Lett.* **46**, 1454-1457.
HEITLER, W. (1949). *The Quantum Theory of Radiation*, 2nd ed. Oxford Univ. Press.
HILDEBRANDT, G., STEPHENSON, J. D. & WAGENFELD, H. (1973). *Z. Naturforsch. Teil A*, **28**, 588-594.
International Tables for X-ray Crystallography (1968). Vol. III. Birmingham: Kynoch Press. (Present distributor D. Reidel, Dordrecht.)
JONES, H. (1975). *The Theory of Brillouin Zones and Electronic States in Crystals.* Amsterdam: North-Holland.
LAUE, M. VON (1960). *Röntgenstrahl-Interferenzen.* Frankfurt/Main: Akademische Verlagsgesellschaft.
LÖWDIN, P. O. (1956). *Adv. Phys.* **5**, 1-172.
MIJNARENDS, P. (1977). *Compton Scattering*, edited by B. WILLIAMS, pp. 323-345. New York: McGraw-Hill.
SCHÜLKE, W. (1981). *Phys. Lett. A*, **83a**, 451-454.
SCHÜLKE, W. (1982). *Solid State Commun.* **43**, 863-866.
SCHÜLKE, W., BONSE, U. & MOURIKIS, S. (1981). *Phys. Rev. Lett.* **47**, 1209-1212.
SCHÜLKE, W., MOURIKIS, S. & LIEDTKE, K. D. (1984). *Nucl. Instrum. Methods*, **222**, 266-269.
SCHÜLKE, W. & NAGASAWA, H. (1984). *Nucl. Instrum. Methods*, **222**, 203-206.
WAGNER, H. (1956). *Z. Phys.* **146**, 127-168.

Acta Cryst. (1986). A**42**, 98-101

Homometric Polytypes in Cadmium Iodide

BY K. FICHTNER

Central Institute of Physical Chemistry, Academy of Sciences of the GDR, Rudower Chaussee 5, *DDR*-1199 *Berlin, German Democratic Republic*

(*Received* 16 *April* 1985; *accepted* 22 *August* 1985)

Abstract

Two sufficient criteria on homometric polytypes are derived. They are applied to CdI_2. In addition to the known pairs of homometric structures, infinite sets of other pairs may be constructed. Examples of possible pairs of homometric CdI_2 polytypes for all space groups in CdI_2 are given.

Introduction

Homometrics are two or more structures that are neither congruent nor enantiomorphous, but would give identical diffraction patterns. Examples of homometric structures are to be expected particularly among polytypes. Sufficient conditions have been formulated for MX and MX_2 structures (Dornberger-Schiff & Farkas-Jahnke, 1970; Jain & Trigunayat, 1977; Ohsumi & Nowacki, 1981).

Jain & Trigunayat (1977) have formulated two criteria for MX_2-type structures, a proof of which has been given by Chadha (1981). Firstly, a Zhdanov symbol consisting of only even digits and its literally reversed sequence would be either congruent or else homometric. For CdI_2 and PbI_2 no actual example of this kind may exist because of the restrictions in the arrangement of molecular sheets in these compounds (Wahab & Trigunayat, 1980). Secondly, if a Zhdanov symbol of a structure consists of only 2's and pairs of 1's, then this structure and its literally reversed sequence are either congruent or else homometric. Ohsumi & Nowacki (1981) have given a criterion that permits homometric CdI_2 polytypes to be derived from homometric cyclotomic sets (Patterson, 1944; Buerger, 1976). In the present paper, both the criteria valid for CdI_2 are generalized.

Possible CdI_2 structures, homometric according to one of the known criteria, have space group $P3m1$ or $P6_3mc$. It will be shown that there may also exist pairs of homometric structures with space group $P\bar{3}m1$, $R3m$ and $R\bar{3}m$, respectively. A pair of homometric CdI_2 polytypes with different space groups is constructed.

Two theorems on homometrics among polytypes

Theorem 1. Let P_I be a polytype satisfying the following conditions:

(i) P_I is composed of two kinds of parallel layers S and T;

(ii) the origins of S and T may be chosen such that there is a straight line through the origins of all the layers of P_I.

Let P_{II} be the polytype whose structure is described by the reverse stacking sequence of layers S and T in P_I. Then the structures of P_I and P_{II} are either congruent or enantiomorphic or homometric.

The proof of this theorem is based on formula (1) derived by Marumo & Saito (1972) for layered structures satisfying conditions (i) and (ii).

0108-7673/86/020098-04$01.50